Journal of Zhejiang University-SCIENCE B (Biomedicine & Biotechnology)
ISSN 1673-1581 (Print); ISSN 1862-1783 (Online)
www.zju.edu.cn/jzus; www.springerlink.com
E-mail: jzus@zju.edu.cn

Spatio-temporal reconstruction of air temperature maps and their application to estimate rice growing season heat accumulation using multi-temporal MODIS data*

Li-wen ZHANG[†1,2,3], Jing-feng HUANG[†‡1,2,3], Rui-fang GUO[1,2,3], Xin-xing LI[1,2,3], Wen-bo SUN[4], Xiu-zhen WANG[5]

([1]*Institute of Remote Sensing and Information Application, Zhejiang University, Hangzhou 310058, China*)

([2]*Key Laboratory of Polluted Environment Remediation and Ecological Health, Ministry of Education, College of Natural Resources and Environmental Science, Zhejiang University, Hangzhou 310058, China*)

([3]*Key Laboratory of Agricultural Remote Sensing and Information System of Zhejiang Province, Hangzhou 310058, China*)

([4]*Meteorological Information Technology Support Center of Jilin Province, Changchun 130062, China*)

([5]*Institute of Remote Sensing and Earth Sciences, Hangzhou Normal University, Hangzhou 311121, China*)

[†]E-mail: flowerpapa@hotmail.com; hjf@zju.edu.cn

Received June 14, 2012; Revision accepted Oct. 15, 2012; Crosschecked Jan. 13, 2013

Abstract: The accumulation of thermal time usually represents the local heat resources to drive crop growth. Maps of temperature-based agro-meteorological indices are commonly generated by the spatial interpolation of data collected from meteorological stations with coarse geographic continuity. To solve the critical problems of estimating air temperature (T_a) and filling in missing pixels due to cloudy and low-quality images in growing degree days (GDDs) calculation from remotely sensed data, a novel spatio-temporal algorithm for T_a estimation from Terra and Aqua moderate resolution imaging spectroradiometer (MODIS) data was proposed. This is a preliminary study to calculate heat accumulation, expressed in accumulative growing degree days (AGDDs) above 10 °C, from reconstructed T_a based on MODIS land surface temperature (LST) data. The verification results of maximum T_a, minimum T_a, GDD, and AGDD from MODIS-derived data to meteorological calculation were all satisfied with high correlations over 0.01 significant levels. Overall, MODIS-derived AGDD was slightly underestimated with almost 10% relative error. However, the feasibility of employing AGDD anomaly maps to characterize the 2001–2010 spatio-temporal variability of heat accumulation and estimating the 2011 heat accumulation distribution using only MODIS data was finally demonstrated in the current paper. Our study may supply a novel way to calculate AGDD in heat-related study concerning crop growth monitoring, agricultural climatic regionalization, and agro-meteorological disaster detection at the regional scale.

Key words: MODIS land surface temperature, Air temperature estimation, Reconstruction, Heat accumulation, Rice growing season, Growing degree day (GDD)

doi:10.1631/jzus.B1200169 **Document code:** A **CLC number:** P49

1 Introduction

Heat units or thermal time, introduced by Reaumut in 1730 to explain the relationship between the growth duration and temperature, has been successfully used in a variety of agricultural sciences (McMaster and Wilhelm, 1997). The accumulation of heat units in a region usually represents the local heat resources. As a crucial driving factor to attain a certain phenological stage, those temperature-based agro-meteorological indices expressed in growing

‡ Corresponding author

* Project supported by the National Key Technology R&D Program of China (No. 2012BAH29B02) and the PhD Programs Foundation of Ministry of Education of China (No. 200100101110035)

degree days (GDDs, °C·d), photothermal units (PTU, °C·d), and heliothermal units (HTU, °C·d), are quite useful in agricultural management decisions such as crop growth monitoring, yield prediction, and the detection of phenological developments (Gordon and Bootsma, 1993).

Advances in temporal and spatial resolution and ease of availability have made remotely sensed data derived from the moderate resolution imaging spectroradiometer (MODIS) instrument onboard the Terra and Aqua satellites the most commonly used data sets in agricultural and environmental applications at the regional and global scale. Numerous studies using MODIS products have developed a series of algorithms to carry out crop identification and mapping, phenophase detection, yield estimation (Sun *et al*., 2009), and meteorological disaster monitoring. Studies have shown that temperature-based agro-meteorological indices such as GDD, have vastly improved the precision of phenological event identification (McMaster and Wilhelm, 1997; Vina *et al*., 2004; Boschetti *et al*., 2009) and models of yield estimation (Teal *et al*., 2006; Sarma *et al*., 2008).

Traditionally, temperature based thermal indices are available from the point calculation of field observations of near surface air temperature (T_a, usually 1.5 m higher than the ground) from a limited number of meteorological stations. A few previous studies paid attention to the methodology for rasterizing accumulated heat units based on the Geographic Information System (GIS) interpolation (Liu *et al*., 2011; Ye *et al*., 2011) at the regional scale with the conventional methods such as kriging and inverse distance weighting (IDW) and modified IDW method improved by digital elevation model (DEM) (Li *et al*., 2010). However, these indices are usually irregularly and sparsely distributed or unavailable from areas in complex terrain without meteorological stations; traditional geospatial interpolation approaches perform unreliably for some big and continuous scale models. Additionally, their results contain lots of uncertainty since the quality of interpolation is very much a function of the method employed (Hassan *et al*., 2007a). Alternatively, the thermal images from remotely sensed satellites, usually give better spatial results (Florio *et al*., 2004). MODIS provides an abundant series of land surface temperature (LST) products with different spatial and temporal resolutions from both Terra and Aqua platforms. The spatiotemporal patterns of MODIS LST-based GDD maps can preserve microhabitat-like effects better than interpolation maps from meteorological data (Neteler, 2010). There are some previous studies that try to carry out such mapping of agro-meteorological indices by remotely sensed LST data. Hassan *et al*. (2007a) listed several previous studies providing long-term expression of GDD on the relationship between remotely sensed normalized difference vegetation index (NDVI) time series and GDD. Instead of this GDD-VI approach, Hassan *et al*. (2007b) focused on the methods using MODIS-based LST to calculate spatially continuous GDD maps at different spatial scales. Zorer *et al*. (2011) calculated accumulative Winkler Index (WI) or GDDs maps derived from aggregated daily MODIS LST of Terra and Aqua satellites to assess their suitability for viticulture of the region.

However, this work largely neglects the problem that the temperature in GDD calculations is designed by T_a but not LST, which probably accounts for the over-estimation of remotely sensed index values relative to the true ground values. Mapping GDD from remotely sensed data, in actuality, is equal to mapping maximum and minimum T_a. At present, MODIS LST has been used, with some difficulty, to estimate minimum and maximum near-surface T_a with several categories of methods such as the statistic regression method, artificial neural network models, the temperature-vegetation index (TVX) method, and a method based on surface energy balance. Among those methods, the statistical method, often linking LST and other geographical parameters such as latitude, longitude, and continentality (distance from the sea), has been a classical and most accurate approach to model maximum and minimum T_a at a local scale (Mostovoy *et al*., 2006; Cristóbal *et al*., 2008; Vancutsem *et al*., 2010). Another problem in calculating GDD by optical remotely sensed data is the missing values due to clouds and other reasons. The reconstruction of T_a maps is necessary to ensure the accuracy of long time accumulations. Some spatial interpolation algorithms such as volumetric spline interpolation (Neteler, 2010; Zorer *et al*., 2011) and temperature gradient-based interpolation (Ke *et al*., 2011) have been used to fill in the missing pixels in LST maps. A more complex method of filling gaps

can be performed on the basis of the surface energy balance equation which estimates the cloudy pixel values from neighboring clear day pixels (Lu *et al*., 2011). Actually, clouds move over time, which makes merging multi-temporal satellite (e.g., Terra and Aqua platform) data with high temporal resolution an effective solution for the problem of missing pixels (Coops *et al*., 2007; Crosson *et al*., 2012).

The objectives of the current study are as follows: (1) to provide a methodology taking advantage of the complementarity of the Terra and Aqua platform to spatio-temporally reconstruct maximum and minimum T_a maps derived from MODIS LST data; (2) to evaluate the feasibility of employing accumulative growing degree day (AGDD) anomaly maps to characterize the 2001–2010 spatial and temporal variability of heat accumulation during the rice growing season in Jilin Province, China, and estimating the 2011 heat accumulation distribution using only MODIS data.

2 Materials and methods

2.1 General description of study region

The study region, Jilin Province, is situated in the centre of Chinese northeast region between 40°52′–46°18′ Latitude N and 121°38′–131°19′ Long E (Fig. 1). It has a temperate continental monsoon climate which features four distinct seasons with a hot rainy season, and receives an annual precipitation ranging from 400 to 600 mm. The annual mean air temperature is between 2–6 °C and an annual average sunshine duration of 2259–3016 h. The landforms vary from western plains and central low hills to the eastern high mountains, with altitudes ranging from 4 m along the Tumen River to 2691 m on Changbai Mountain. The district's vertical climate zone supports many types of vegetation including meadow, crops, and needle\broad-leaved forest. Rice is the main food crop grown in Jilin Province, with a growing season of April to September. Therefore, the current study only assesses the local heat condition during this period of time.

2.2 Available data and pre-processing

In this paper, the details of available data sources with remotely sensed, meteorological and other geographic data were listed in Table 1. The four categories of MODIS data, namely 8-d LST/emissivity 1000 m products (MOD/MYD11A2.005), 8-d surface reflectance 500 m product (MOD09A1.005), and yearly land cover 500 m product (MCD12Q1.005) were from the NASA Terra and Aqua satellites. The data were downloaded from NASA FTP site spanning the years of 2001–2011 (2001–2010 for model and 2011 for verification). For each year a total of 22 8-d composites of all products (from the 105th day of year (DOY_{105}) to DOY_{273}) were used. The MODIS

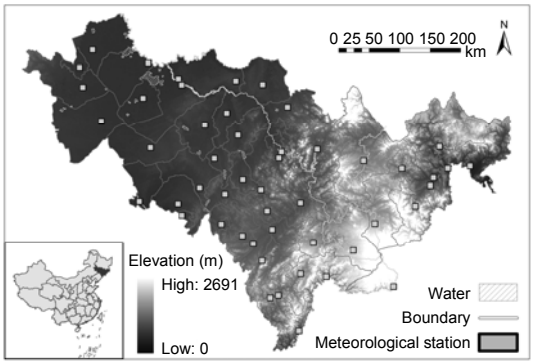

Fig. 1 Location and elevation of study region, Jilin Province, China
The distribution of a total of 50 meteorological stations is labeled with small white squares

Table 1 Summary of available data in current study

Data type		Original resolution	Utility	Source
MODIS products	MOD11A2	8 d, 1000 m	Max/min T_a estimations and GDD/AGDD calculations	http://lpdaac.usgs.gov/lpdaac/products
	MYD11A2	8 d, 1000 m		
	MOD09A1	8 d, 500 m		
	MCD12Q1	Yearly, 500 m	Water mask	
Meteorological temperature data	Maximum	Daily	Precision validation	Jilin Provincial Meteorological Bureau
	Minimum	Daily		
Auxiliary geographic data	ASTER GDEM	30 m	Fitting models	http://asterweb.jpl.nasa.gov/gdem.asp
	Boundaries		Map	http://nfgis.nsdi.gov.cn/

reprojection tool software (MRT V4.0) was used to mosaic and reproject all the MODIS data from HDF format with the original sinusoidal (SIN) to a TIFF file with the Lambert conformal conic projection (SD_1=25, SD_2=47, CM=105, WGS84 ellipsoid). In order to operate calculations at the pixel scale, all MODIS images need to be resampled into 1000 m with the same spatial resolution of LST data by nearest neighbor (NN) resampling, which can better maintain original brightness values of MODIS pixels and have a quicker processing time during reprojection and spatial resampling (Li *et al*., 2009; Neteler, 2010).

The values of the MOD11A2/MYD11A2 LST were calculated by averaging all the valid pixels under clear-sky during each 8-d period. This method may introduce uncertainty due to using clear sky samples to represent actual value from all sky average (Shen and Leptoukh, 2011) However, we selected MODIS 8-d LST to calculate the multi-year heat accumulations during the whole period of the rice growing season mainly for two reasons: (1) Comparing the daily products, 8-d products can minimize the loss of data due to clouds to a large extent, which is essential to retain a more reliable source for the estimation of T_a. (2) There is a high consistency between the two estimations of heat accumulation from meteorological daily T_a and 8-d composited mean T_a with the slopes of linear regression around 1.0 and correlation coefficients over 0.99. It is reasonably assumed that the temporal resolution change of original data from daily to 8-d composition brings little error to the final heat accumulation estimation. Therefore, we chose to characterize the multi-year variation of rice growing season heat accumulation by using less data-intensive 8-d LST products.

Enhanced VI (EVI) time series were first calculated by blue, red, and near infrared bands from MOD09A1 based on the Eq. (1). Then an algorithm proposed by Sun *et al*. (2009) was implemented to remove the cloudy pixels which were identified by the information in the quality assessment (QA) layer. The MODIS land cover type product contains multiple classification schemes, which were derived from observations spanning a year of Terra and Aqua data. In this study, we extracted all water pixels labeled by the plant functional type (PFT) scheme in MCD12Q1 of each year and then aggregated multi-year water pixels into one water mask. All of the MODIS-derived values were extracted from the MODIS pixel where the meteorological stations located. No aggregation technique was used in the current paper since there is a complex elevation gradient in the eastern study area.

The meteorological data for the Jilin Province (daily minimum and maximum temperature) were provided by the Jilin Provincial Meteorological Bureau for the period 2001–2011. Corresponding to the $DOY_{105–273}$ of MOD/MYD11A2 products, we employed the simple average method for daily maximum and minimum air temperature data at 8-d intervals from 50 meteorological stations to compose corresponding 8-d mean maximum air temperature ($T_{a\text{-}max}$) and 8-d mean minimum air temperature ($T_{a\text{-}min}$) for each station over the rice growing season of all 10 years. Additionally, we use the same periods of $T_{a\text{-}max}$ and $T_{a\text{-}min}$ data to calculate 8-d mean meteorological derived GDD (Meteo-GDD) based on Eq. (2), 8-d accumulated Meteo-GDD (Meteo-AGDD) based on Eq. (3), and Meteo-AGDD anomaly based on Eq. (4). All of the above meteorological indices were used for model construction and accuracy verification of corresponding remotely sensed estimated data. It is worth noting that this study found that when DEM data was used, a high correlation with correlation coefficient R=0.923 was observed between 1000 m pixel resolution DEM and actual elevation of 50 meteorological stations. Therefore, the minimal variation of elevation values after being resampled into 1000 m from the original 30 m can be totally ignored during the following model fitting and spatial interpolation.

2.3 Thermal indices and validation index

For this work, annual time series of EVI from DOY_{105} to DOY_{273} were calculated at each pixel from 8-d MOD09A1 data using the formula developed by Huete *et al*. (2002):

$$\mathrm{EVI} = G\frac{\rho_{\mathrm{NIR}} - \rho_{\mathrm{red}}}{\rho_{\mathrm{NIR}} + C_1\rho_{\mathrm{red}} - C_2\rho_{\mathrm{blue}} + L}, \qquad (1)$$

where ρ_{blue}, ρ_{red}, and ρ_{NIR} are blue, red, and near infrared bands in MOD09A1, respectively. For MODIS sensor, L (=1) is the canopy background adjustment, C_1 (=6) and C_2 (=7.5) are aerosol resistance coefficients, and G (=2.5) is a gain factor. Instead of NDVI, we used EVI data as an indicator for analyzing the impacts of

vegetation coverage on the relationship between near surface air temperature and LST since EVI exhibits sensitivity across high vegetation densities and atmospheric effects, and shows better performance in the downscaling study of GDD maps (Hassan *et al*., 2007a). The reason why we selected an 8-d surface reflectance product to calculate EVI rather than directly employing the 16-d composited EVI product (MOD13Q1) was because the former product has the same temporal resolution of 1000 m with 8-d LST product.

There are numerous modified expressions on the basis of the original concept of GDD. In recent years, an increasing number of scientists have defined GDD as the daily thermal-time above the base temperature for plant growth (McMaster and Wilhelm, 1997; de Beurs and Henebry, 2004; Vina *et al*., 2004; Sarma *et al*., 2008), and have taken AGDDs as the index representing heat summation during the whole growing period (Yang *et al*., 1997; Wang *et al*., 2001; Vina *et al*., 2004; de Beurs and Henebry, 2010). In the current paper, 8-d mean GDD (°C·d) was calculated by using the canonical GDD equation from McMaster and Wilhelm (1997):

$$\begin{aligned} &\mathrm{GDD}_t = (T_{\max\text{-}t} + T_{\min\text{-}t})/2 - T_{\mathrm{base}}, \\ &T_{\mathrm{base}} \le T_{\max} \le T_{\mathrm{upper}}, \\ &T_{\mathrm{base}} \le T_{\min} \le T_{\mathrm{upper}}, \end{aligned} \tag{2}$$

where $T_{\max\text{-}t}$ is reconstructed complete $T_{\max}$ (8-d mean maximum air temperature estimated from the MODIS daytime LST image) at DOY_t, $T_{\min\text{-}t}$ is reconstructed complete $T_{\min}$ (8-d mean minimum air temperature estimated from the MODIS nighttime LST image) at the same period. T_{base} is the minimum temperature threshold for crop growth, which varies among species. T_{upper} is the maximum temperature threshold for crop growth. Usually 10 °C is the base temperature for thermophilous crops such as rice (Islam and Sikder, 2011); therefore 10 °C is set to be the base temperature and 40 °C as the upper limit in the current study. When calculating GDD, the following adjustments were carried out: $T_{\min}$ is set to equal to T_{base} if $T_{\min}$ is lower than T_{base}, and set to T_{upper} if $T_{\min}$ is higher than T_{upper}, while $T_{\max}$ is set to equal to T_{base} when lower than T_{base} and equal to T_{upper} when higher than T_{upper}.

To simplify the equation, the quantity $[(T_{\max}+T_{\min})/2]$ is sometimes used instead of daily mean air temperature (Morrison *et al*., 1989; McMaster and Wilhelm, 1997). However, there was no significant variation between the two interpretations of GDD equation during the period of crop growth, and the equation with $T_{\max}$ and $T_{\min}$ used in this paper is the most commonly used for application in crop study since it can remove impacts on the crop growth from extreme high and low air temperature (McMaster and Wilhelm, 1997).

We accumulated each 8-d interval GDDs over the growing season by simple summation when GDD exceeded the base of 10 °C by the equation from de Beurs and Henebry (2004):

$$\mathrm{AGDD}_t = \mathrm{AGDD}_{t-8} + 8 \times \mathrm{GDD}_t, \tag{3}$$

where GDD_t is the 8-d AGDDs at DOY_t and AGDD_t is the GDDs accumulated from the beginning of the time period till DOY_{t+7}. GDD calculated by $T_{\max}$ and $T_{\min}$ images at DOY_t only means the average GDD for 8 d during the period of $\mathrm{DOY}_{t \text{ and } t+7}$. Therefore, every pixel in each GDD image needed to be multiplied by 8 first when it was accumulated into AGDD, which can express the meaning that AGDD is the summation of daily GDD. In this paper, we accumulate GDDs by beginning with DOY_{105} and ending with DOY_{280}. When GDD_t was greater than zero, AGDD_t was added, otherwise it was ignored. Based on the formula, if we choose 10 °C for rice physiology lower limit temperature as the base temperature in GDD, the value of AGDD is equal to the value of effective accumulative temperature spending 10 °C (de Beurs and Henebry, 2004).

AGDD anomaly (AGDD_a) indicates the departure from one year AGDD to the multi-year average level. The equation of AGDD anomalies is as given below:

$$\mathrm{AGDD}_{ai} = \mathrm{AGDD}_i - \overline{\mathrm{AGDD}}, \tag{4}$$

where AGDD_{ai} is AGDD anomaly at the year of i, AGDD_i is accumulated GDDs from DOY_{105} to DOY_{273} at the same year, $\overline{\mathrm{AGDD}}$ is the average of 10 years AGDD from DOY_{105} to DOY_{273}.

The consistency between all the meteorological data and corresponding remotely sensed estimated

data is evaluated by the mean bias error (MBE), mean absolute error (MAE), and root mean squared error (RMSE).

The MBE is given by:

$$\mathrm{MBE}=\frac{\sum_{i=1}^{n}(x_i-y_i)}{n}, \tag{5}$$

where x_i and y_i are the measured and estimated values from meteorological station and MODIS data, respectively, and n is the number of data pairs. In the study, MBE can explain the average over or underestimation of estimated data from the true value.

The MAE and RMSE are given by:

$$\mathrm{MAE}=\frac{\sum_{i=1}^{n}|x_i-y_i|}{n}, \tag{6}$$

$$\mathrm{RMSE}=\sqrt{\frac{\sum_{i=1}^{n}(x_i-y_i)^2}{n}}. \tag{7}$$

As the name suggests, the MAE is an average of absolute errors and the RMSE is a quadratic scoring rule which measures the average magnitude of the errors. In statistics, both quantities are used to measure how close predictions or estimation are to the true observation, with RMSE giving a relatively high weight to large errors. The parameters of these two equations are the same as those for MBE. Usually, lower values are desirable.

2.4 Data processing steps

The details of the algorithm in this study are shown in Fig. 2. The five main steps were hereinafter described in sequence.

The first step is the filtering of low-quality quality control (QC) values due to clouds or other processing failures of each of the LST images. The QC SDSs for LST and emissivity provide quality information on algorithm results for each pixel, which can be extracted by reading the bits in the 16-bit unsigned integer (Wan, 2007). We determined the good quality (valid) LST pixels according to the following criteria: mandatory QA flags=pixel produced, good quality; data quality flag=good; emissivity flag=average emissivity error ≤0.01; LST error flag: 00=average LST error ≤1K. Only those good quality pixels were used for model fitting. After quality filtering and converting LST values from Kelvin to Celsius ($\mathrm{LST_C}=\mathrm{LST_K}\times 0.02-273.15$), to link the $\mathrm{LST_{Day}}$/$\mathrm{LST_{Night}}$, EVI, and elevation with actual maximum/minimum T_a from meteorological stations by multiple stepwise regression analysis, the optimal regression model with biggest adjusted R^2 value was applied to estimate fitted daytime and nighttime T_a maps from Terra and Aqua platforms, respectively.

The third step was the temporal merging of fitted T_a maps at each 8-d period. For the year of 2003–2010, the 8-d synthetic maximum air temperatures (T_{max}) were merged from two fitted daytime T_a maps ($T_{max\text{-}Terra}$ and $T_{max\text{-}Aqua}$) of the same 8-d period. For example, the T_{max} map of $\mathrm{DOY_{105}}$ is the merging result of $T_{max\text{-}Terra}$ of $\mathrm{DOY_{105}}$ and $T_{max\text{-}Aqua}$) of $\mathrm{DOY_{105}}$. The algorithm of temporal merging is as follows: for a given pixel, if both input maps have the fitted values, the value of the synthetic T_{max} map is the average of $T_{max\text{-}Terra}$ and $T_{max\text{-}Aqua}$. If only one of two fitted values was present in the maps, that single value was used. Otherwise, if neither of the two maps had the fitted values, it was kept as an invalid value and was set aside for filling by spatial interpolation in the next step. Similar algorithms were carried out to produce the synthetic T_{min} map from $T_{min\text{-}Terra}$ and $T_{min\text{-}Aqua}$ images of the same 8-d period. It is worth mentioning that temporal merging from two platforms was not implemented for the T_{max} and T_{min} maps of 2001 and 2002 since we could only acquire the complete available data of Terra satellite before 2003; therefore, for 2001–2002, T_{max} and T_{min} were directly substituted by daytime fitted $T_{max\text{-}Terra}$ and nighttime fitted $T_{min\text{-}Terra}$, respectively.

The residual invalid pixels presenting in the synthetic T_{max} and T_{min} images were spatially interpolated with an algorithm inspired by Neteler (2010) which is based on regression analysis between surface temperature and elevation in each sliding window of the original image. If there were more than 10% valid T_a pixels per sliding window and existing a regression relationship built by those 10% valid T_a with corresponding DEM, the remaining invalid pixels will be filled by this regression relationship with DEM, otherwise it skipped to the next sliding window. This process was implemented until all the invalid pixels

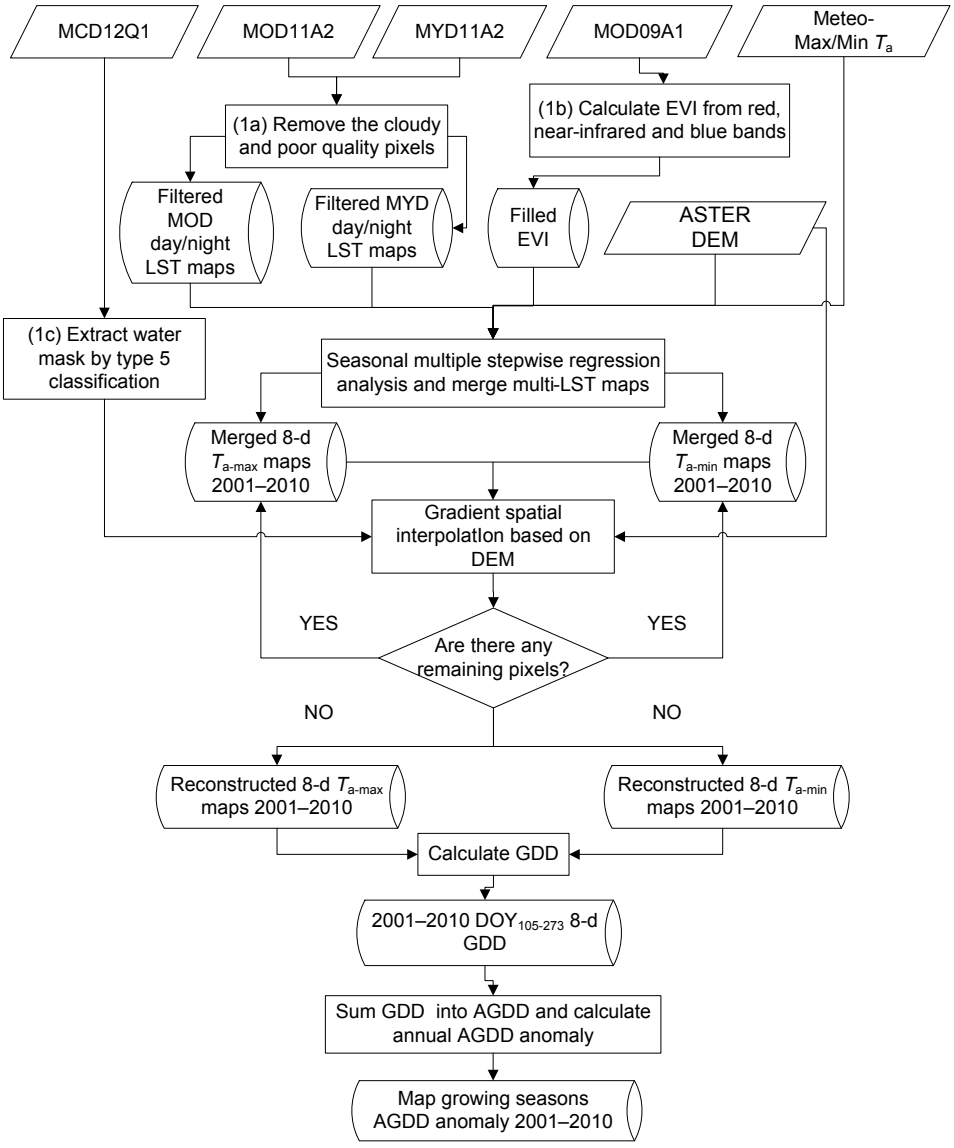

Fig. 2 Flowchart to estimate GDD and annual AGDD anomaly maps from multi-temporal MODIS LST data

of whole image were filled. Twenty-four pixels were taken as the best sliding window radius in the current paper after the repeated test. More algorithm details can be seen in the literature (Neteler, 2010; Ke *et al*., 2011).

Finally, GDD and AGDD and AGDD anomaly were calculated by using synchronous completely reconstructed T_{max} and T_{min} for every 8-d period in the rice growing season of each year, and then verified against corresponding ground meteorological stations' data.

3 Results

3.1 Maximum and minimum T_a estimation and model validation

The basic mechanism for estimating air temperatures with remotely sensed LST relies on the intense heat exchange between land surface and atmosphere. In this study, air temperature was modeled as a function of EVI, elevation, and MODIS LST. Given the seasonality effect of the relationship between T_a and LST, models were established for four different

remotely sensed LST data across three seasons during the rice growing season. Thus, a total of 12 regression models were created for each of $LST_{Day\text{-}Terra}$, $LST_{Night\text{-}Terra}$, $LST_{Day\text{-}Aqua}$, and $LST_{Night\text{-}Aqua}$ for three different seasons, corresponding to data from 50 meteorological stations which were listed in Table 2. On the whole, compared with Aqua, RMSE of maximum air temperature (T_{max}) modeled by Terra daytime LST was lower, the same as minimum air temperature (T_{min}) modeled by Terra nighttime LST.

Some literature also pointed out that T_a estimated from Terra MODIS LST data has a smaller deviation with ground observation than the estimation derived from Aqua MODIS LST data (Zhang *et al*., 2011). For 40% of the test samples, seasonal statistics show the lowest RMSE value of 1.780 and 1.958 °C in Terra and Aqua fall models for T_{max} estimation and 1.554 and 1.598 °C in summer models for T_{min} estimation. Spring models showed the poorest performance in estimating both T_{max} and T_{min} from Terra and Aqua daytime/nighttime LSTs.

3.2 Reconstruction of estimated T_a maps and accuracy validation

3.2.1 Temporal merging of T_{max} and T_{min} from Terra and Aqua T_a estimation

There is a large amount of temporal and spatial missing pixels accounted for by clouds and low quality in LST data (Crosson *et al*., 2012). Here, we introduced a spatio-temporal algorithm to fill those gaps in estimated T_a images with two main strategies: firstly, temporally merged images of two acquired times and secondly, spatially interpolated in the current merged image. The object of this two-steps reconstruction for estimated T_a images over the entire study area was to deal with the significant problem of missing data in determining GDDs. The performance of the temporal reconstruction was illustrated in Fig. 3. For the DOY_{105} of 2003, the $T_{max\text{-}Terra}$ image shows the pattern of T_{max} with large invalid areas (cloudy area and an area with a large LST retrieval error) in the southeast and smaller regions in the central area,

Table 2 Seasonal regression models of statistical estimation of 8-d mean maximum and minimum air temperatures from MODIS LST data over the Province of Jilin over all types of land cover

Type	Season	Model	T_a			n	
			Adjust R^2	RMSE-fit	RMSE-test	Fit 60%	Test 40%
$T_{max\text{-}Terra}$	Spring	T_{max}=3.473+0.568LST+12.268EVI	0.573**	2.712	2.674	1 006	670
	Summer	T_{max}=15.935+0.347LST+4.469EVI−0.002Elevation	0.367**	2.010	2.040	1 706	1 138
	Fall	T_{max}=4.488+0.674LST+8.702EVI	0.709**	1.610	1.780	1 133	755
$T_{min\text{-}Terra}$	Spring	T_{min}=0.293+0.832LST+3.615EVI−0.003Elevation	0.777**	1.663	1.570	976	651
	Summer	T_{min}=3.339+0.742LST+2.592EVI−0.002Elevation	0.723**	1.452	1.554	1 568	1 045
	Fall	T_{min}=0.608+0.809LST+3.464EVI−0.003Elevation	0.792**	1.593	1.685	855	570
$T_{max\text{-}Aqua}$	Spring	T_{max}=4.508+0.495LST+10.588EVI	0.473**	2.920	3.017	612	409
	Summer	T_{max}=19.642+0.237LST+2.666EVI−0.002Elevation	0.271**	2.106	2.162	1 054	703
	Fall	T_{max}=7.452+0.519LST+8.240EVI−0.002Elevation	0.575**	1.885	1.958	728	485
$T_{min\text{-}Aqua}$	Spring	T_{min}=4.658+0.754LST+3.034EVI−0.003Elevation	0.762**	1.985	1.898	1 054	702
	Summer	T_{min}=8.086+0.613LST+1.257EVI−0.004Elevation	0.667**	1.665	1.598	850	566
	Fall	T_{min}=2.184+0.757LST+5.841EVI−0.004Elevation	0.743**	1.720	1.858	772	515

Models were assessed based on coefficient of determinations (R2) and RMSE of fitting and test data, respectively. ** Significance at $p<0.0001$. Referring to the season category reported by Crosson *et al*. (2012), period of DOY of 105–145 (March to May) is considered 'spring', DOY of 153–233 (June to August) is 'summer', and DOY of 241–280 (September to November) is 'fall'. Models based on Terra LST are estimated by all the data from 10 years (2001–2010) for each season. Models based on Aqua LST are estimated by all the data from eight years (2003–2010) for each season

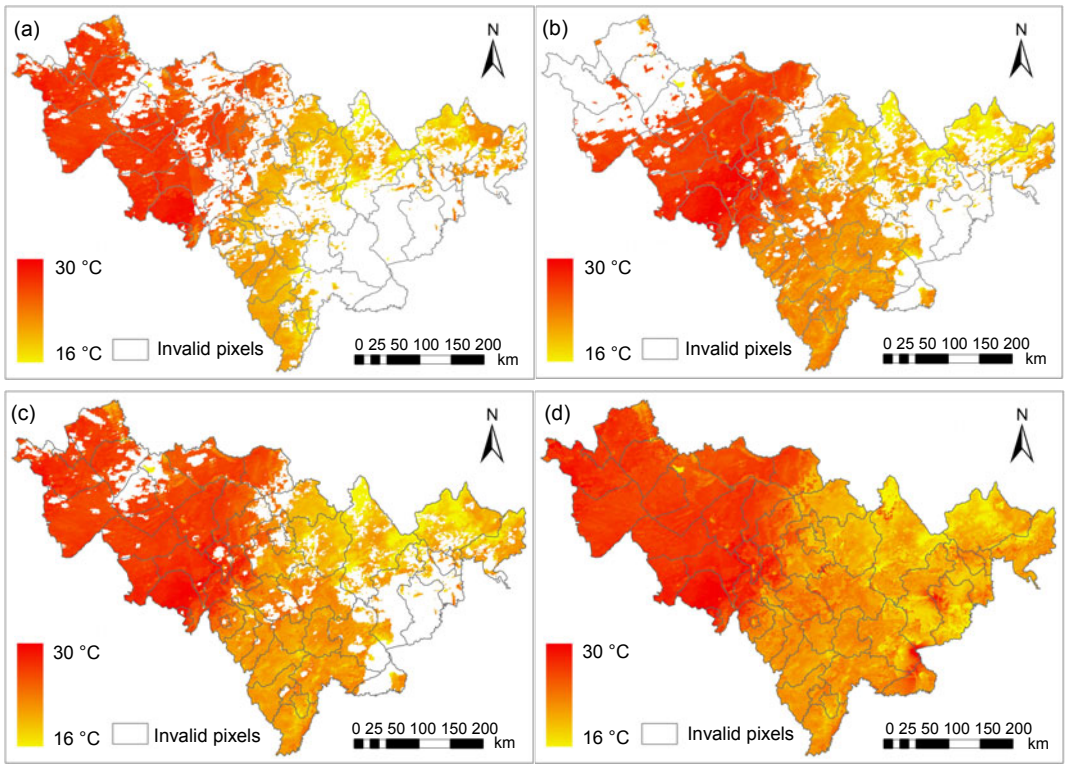

Fig. 3 Differences between original filtered T_{max} maps for Terra (a) and for Aqua (b), merged T_{max} map (c) and reconstructed complete T_{max} map (d) for DOY_{105} in 2003
Areas of water and missing data (invalid pixels) are in white

while the $T_{max\text{-}Aqua}$ image displays the pattern of T_{max} with a large invalid area in the northwest and smaller regions in the east. After merging $T_{max\text{-}Terra}$ (Fig. 3a) and $T_{max\text{-}Aqua}$ (Fig. 3b) into T_{max} (Fig. 3c), there was a small area of concentrated invalid pixels allocated in the eastern region. We assure that the temporal merging of maps from Terra and Aqua platforms can introduce higher quality T_a pixels reflecting true temperature values when the cloudy condition varies quickly between two satellite's overpass times. After this temporal merging step, the remaining pixels present in the synthetic images were spatially interpolated with an algorithm based on the relationship between surface temperature and elevation in each sliding window on the original image (Neteler, 2010), then a series of complete T_{max}/T_{min} images were reconstructed. The Fig. 3d showed the eventual result after two-step reconstructions.

We defined the percentage of valid air temperature pixels out of the complete number of pixels covering the study area as the coverage rate. Thus, a coverage improvement rate means an increased pecentage of valid pixels from either the Terra-based T_a map or the Aqua-based T_a map as compared to the temporal-merged T_a map. The coverage improvement rate of temporally merged T_{max}/T_{min} images from Terra/Aqua T_{max}/T_{min} and eventual average coverage rate of merged T_{max}/T_{min} were displayed in Table 3. Because the Aqua MODIS data of the rice growing season can only be completely acquired from 2003 onwards, we only compared the coverage improvement rate for the years of 2003–2010. Generally, data from satellite images taken in the afternoon are more frequently interrupted by cloud, therefore it is not surprising that Table 3 reveals a remarkably better improvement for Aqua platform than for Terra platform, with annual average coverage improvement rate ranges of 5.60%–7.22% for $T_{max\text{-}Terra}$, 9.56%–14.53% for $T_{max\text{-}Aqua}$, 4.84%–5.86% for $T_{min\text{-}Terra}$, and 13.85%–17.72% for $T_{min\text{-}Aqua}$ images over eight years. Eventually, the average spatial coverage during the rice growing season for eight years could reach 84.07% for merged T_{max} image and 85.54% for merged T_{min} image. For seasonal analysis (Fig. 4), the improvement was the most significant for the summer season with the average spatial coverage

increasing from 70.37% and 64.43% of $T_{max\text{-}Terra}$ and $T_{max\text{-}Aqua}$ respectively to 78.03% of merged T_{max} image, 69.70% and 55.98% of $T_{min\text{-}Terra}$ and $T_{min\text{-}Aqua}$ to 76.50% of the merged T_{min} image, 86.28% and 95.90% for spring merged T_{max} and T_{min} images, and 91.65% and 94.13% for fall T_{max} and T_{min}. After carrying out the temporal merging, it is easier to fill in the remaining invalid pixels by interpolation based on temperature gradient.

3.2.2 Precision validation of T_{max} and T_{min} estimation

We spatially interpolated the remaining pixels by adjacent good quality (clear-day) pixels. This method may introduce uncertainty since cloudy areas may have had lower solar irradiation and T_a than clear areas. However, it is an inevitable defect of optical remote sensing that the accurate estimation of some pixels will be impossible due to cloud cover. In the current paper, we only focus on the supposition whether or not the reconstructed T_a can be taken as a proxy for real T_a to estimate the heat accumulation. To clarify how many errors were introduced in each different reconstruction steps, the precision validations of all pixels in each 8-d T_{max} and T_{min} image were calculated respectively for the following two categories: good pixels and invalid pixels. Good pixels are those T_a estimation pixels from LST data after QC filter and temporal merging, which can be taken as the high quality T_a pixels of clear sky. The invalid pixels are the remaining pixels from cloudy sky and low quality in the product and are filled by the spatial interpolation.

It could be seen in Tables 4 and 5 that statistic regression and temporal merging brought a total

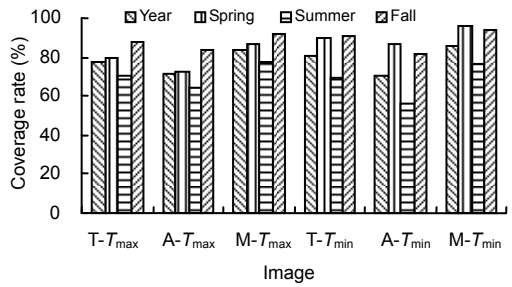

Fig. 4 Comparison of seasonal and annual mean coverage rate of T_{max} and T_{min} images from Terra and Aqua platform and their temporal merging

T-T_{max}, A-T_{max}, and M-T_{max} are $T_{max\text{-}Terra}$, $T_{max\text{-}Aqua}$, and temporally merged T_{max} images, so T-T_{min}, A-T_{min}, and M-T_{min} the corresponding T_{min} images

Table 3 Coverage improvement rate of temporally merged T_{max} and T_{min} images

Year	CIR (%)				CR (%)	
	T-T_{max}	A-T_{max}	T-T_{min}	A-T_{min}	M-T_{max}	M-T_{min}
2003	7.17	13.95	4.93	16.37	86.44	84.86
2004	5.81	9.56	4.84	13.85	84.26	85.65
2005	7.22	13.54	5.05	16.15	78.98	82.05
2006	6.48	11.77	5.12	15.19	83.10	84.86
2007	5.89	11.35	5.86	14.58	86.68	87.64
2008	6.51	14.53	5.18	16.12	85.42	90.23
2009	5.60	11.79	5.18	14.52	85.35	86.42
2010	7.09	12.55	5.04	17.72	82.30	82.59
Mean	6.47	12.38	5.15	15.56	84.07	85.54

CIR: coverage improvement rate; CR: coverage rate. T-T_{max}, A-T_{max}, and M-T_{max} are $T_{max\text{-}Terra}$, $T_{max\text{-}Aqua}$, and temporally merged T_{max} images, so T-T_{min}, A-T_{min}, and M-T_{min} the corresponding T_{min} images

Table 4 Precision validation of T_{max}

Year	Good pixel			Invalid pixel			All pixel	
	MBE (°C)	RMSE (°C)	n	MBE (°C)	RMSE (°C)	n	MBE (°C)	RMSE (°C)
2001	1.77	2.87	743	3.32	4.73	335	2.25	3.55
2002	1.56	3.01	675	1.91	3.80	403	1.69	3.33
2003	1.68	3.03	778	2.05	3.46	300	3.46	3.16
2004	1.57	2.68	761	1.85	3.19	317	1.65	2.84
2005	1.10	2.91	681	1.71	3.06	397	1.33	2.97
2006	1.66	3.11	766	1.78	3.58	312	1.70	3.25
2007	1.46	2.59	786	1.97	3.36	292	1.60	2.82
2008	1.40	2.90	804	1.82	3.36	274	1.51	3.03
2009	1.44	3.17	792	0.15	3.54	286	1.10	3.27
2010	1.18	2.39	727	1.59	3.43	351	1.31	2.77
Mean	1.48	2.87		1.82	3.55		1.76	3.10

Table 5 Precision validation of T_{min}

Year	Good pixel			Invalid pixel			All pixel	
	MBE (°C)	RMSE (°C)	n	MBE (°C)	RMSE (°C)	n	MBE (°C)	RMSE (°C)
2001	0.48	1.65	725	2.16	2.71	353	1.03	2.06
2002	0.44	2.05	729	1.58	2.28	349	0.81	2.12
2003	0.30	1.77	820	1.66	2.34	258	0.62	1.92
2004	0.05	1.85	853	1.86	2.46	225	0.42	1.99
2005	0.61	1.75	783	2.49	3.08	295	1.12	2.19
2006	0.16	1.62	834	1.86	2.56	244	0.54	1.88
2007	0.21	1.72	863	1.99	2.60	215	0.56	1.93
2008	0.19	1.71	892	1.82	2.60	186	0.47	1.89
2009	0.25	1.63	849	1.77	2.45	229	0.57	1.84
2010	0.26	1.74	803	2.52	3.17	275	0.84	2.19
Mean	0.29	1.75		1.97	2.62		0.70	2.00

underestimation for maximum T_a with 10-year mean MBE in 1.48 °C and quite few underestimations for minimum T_a with a mean MBE in 0.29 °C. While these underestimations further increased after spatial interpolation, the 10-year mean MBEs for invalid pixels of T_{max} and T_{min} were 1.82 and 1.97 °C, while RMSE increased from 2.87 to 3.55 °C and 1.75 to 2.63 °C, respectively. However, the reconstruction effects of T_{max} and T_{min} during the whole rice growth season were satisfied with the 2001–2010's RMSE varying from 2.77 to 3.55 °C for T_{max} and 1.84 to 2.19 °C for T_{min}.

The comparisons between time series of meteorological and MODIS-derived maximum and minimum air temperature at each 8-d period are shown in Fig. 5. To reflect the overall level of the study area, the values in the curves were the averages of T_a values at each 8-d interval from 50 meteorological stations and the 50 MODIS pixels corresponding to the stations' positions. Overall, the reconstructed estimation of minimum temperature fitting was better than the maximum temperature fitting. It can be seen from the Fig. 5b that 10-year fitted T_{min} from MODIS data basically had a consistent pattern with the $T_{a\text{-}min}$ measured by meteorological stations, except for a tiny discrepancy in the peak of every year. Obviously, T_{min} estimations are quite good in spring and autumn and acceptable in the summer of each year; the average MAEs of all 10 years for spring, summer and fall season are 0.944, 1.231, and 0.917 °C, respectively. However, two almost overlapping curves showed the fact that T_{min} was capable of actually reflecting $T_{a\text{-}min}$. By contrast, difference curve from meteorological $T_{a\text{-}max}$ minus MODIS-derived T_{max} had a larger fluctuation over the "0" value line (Fig. 5a). Ten-year average MAE between T_{max} and $T_{a\text{-}max}$ ranges from 1.697 to 2.541 °C, with 2.592 °C for 'spring days', 1.648 °C for 'summer', and 2.446 °C for 'fall', respectively. The time series of $T_{a\text{-}max}$ and T_{max} basically raised and declined synchronously during the whole 10 years, except when there is a sudden drop of actual weather change.

The complex effects of vegetation cover on the heat exchange between LST and near surface air temperature can probably account for the discrepancies between meteorological observation and MODIS

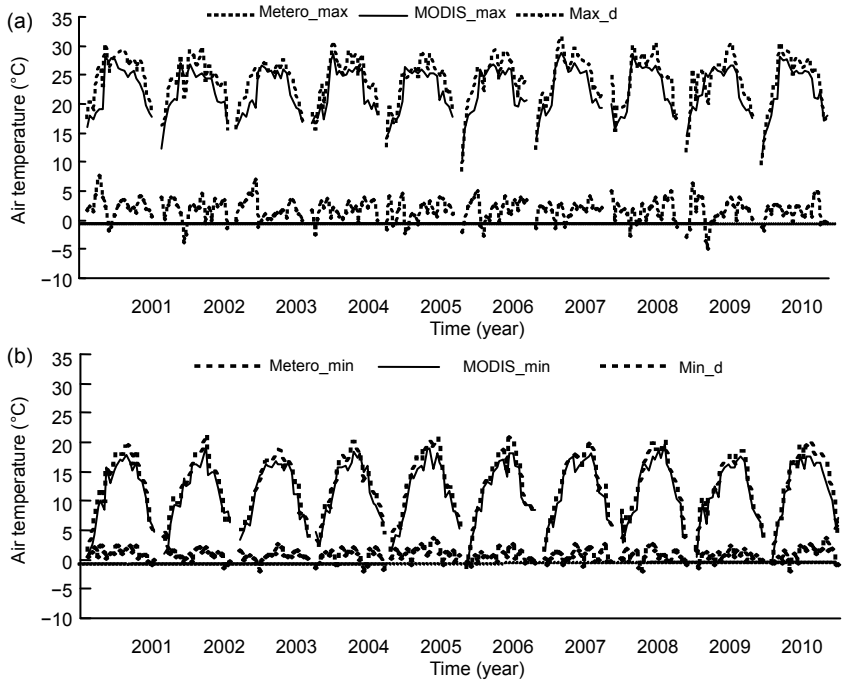

Fig. 5 Comparisons of time series between meteorological and MODIS-derived maximum air temperature (a) and minimum air temperature (b)

The values in curve are the average of 50 meteorological stations at each 8-d intervals during the whole growing season which begins with DOY_{105} and ends with DOY_{273}. Difference curves (max_d and min_d) are the result of meteorological T_a time series minus MODIS-derived T_a time series. The little breaks in the curves represent the time gaps between every year's growing seasons

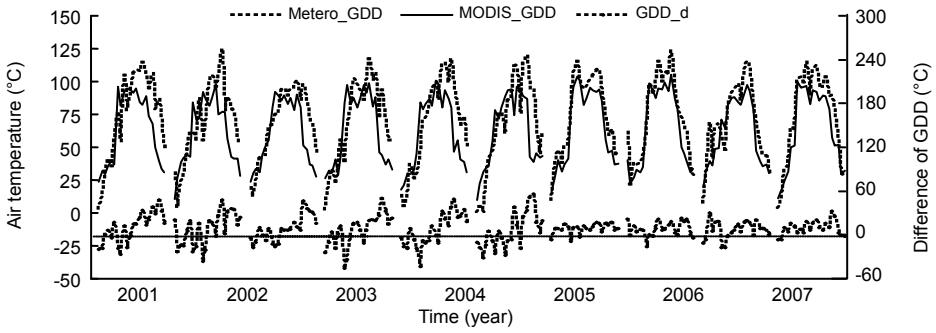

Fig. 6 Average GDD summation of every 8-d intervals from DOY_{105} to DOY_{273} spanning the year of 2001–2010
Difference curve is the result of Meteo-GDD time series minus MODIS-derived GDD time series. The little breaks in the curves represent the time gaps between every year's growing seasons

estimation. Another potential explanation is the possible situation of one or many of the meteorological stations near residential areas, in which case they would be influenced by the urban heat island.

3.3 Comparing meteorological and MODIS-derived GDDs and AGDDs

The differences between Meteo-GDD and MODIS-GDD at each 8-d period spanning the year of 2001–2010 are shown in the Fig. 6 to analyse the error sources from different 8-d periods. The gap was a comprehensive reflection of the difference between reconstructed T_{max}/T_{min} and ground T_a observation. Fig. 6 displayed that the difference between meteorological and MODIS-derived 8-d GDD summation was relatively large in the fall seasons from 2001–2006 and low from 2007–2010 seasons. The "level off" of MODIS-derived from 8-d GDDs in summertime can be accounted for the "plateau" in estimation of T_{max} from LST.

A comparison between meteorological and MODIS-derived AGDD with the period of entire rice growing season was carried out to display the discrepancy at each 8-d period (Fig. 7). It is clearly that there was quite a good agreement during the earlier period of the growing season in spring and summer time. The MODIS-derived AGDDs become slightly lower than the meteorological-derived AGDDs since the fall with largest error at the end of the growing season with 10-year mean difference of 157.7 °C·d. The same results are found in the statistics in each year of the 2001–2010. The reason for this negative difference is under investigation. However, our result of the annual variation of AGDDs with the DOY is similar to the finding of Neteler (2010), who also demonstrated that AGDDs from reconstructed MODIS LST were systematically slightly lower than those calculations from meteorological stations in the fall time.

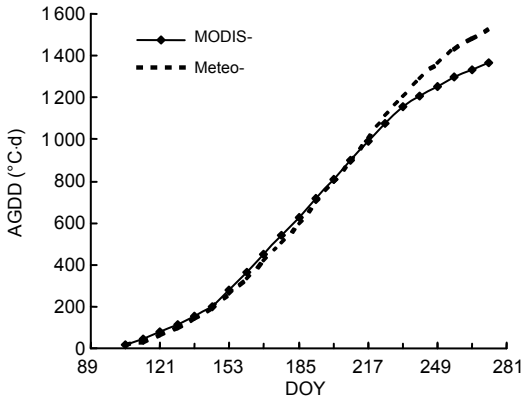

Fig. 7 Comparison of 10-year average AGDDs derived from MODIS data and meteorological stations with the each 8-d period from DOY_{105} to DOY_{273}

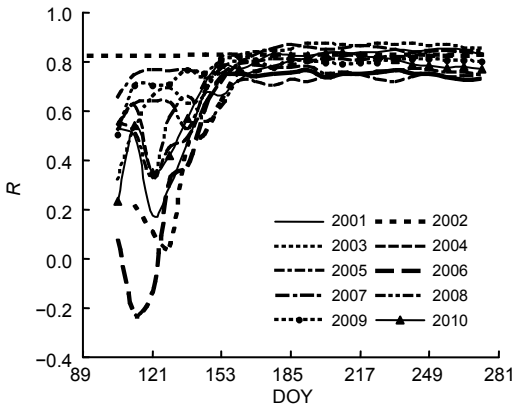

Fig. 8 Correlation coefficient between MODIS-derived and meteorological AGDDs of 50 stations in each 8-d period during the year of 2001 to 2010

Except for the overall comparison, the correlation coefficient between meteorological and remotely sensed AGDDs estimation of 50 stations in every 8-d periods is also analyzed (Fig. 8). The result showed that the correlation coefficients of AGDDs in the spring stage were unstable among ten years with relatively low values. This is probably because the air temperature in spring time is apt to experience a recovering warm fluctuation of around 10 °C, which is difficult to capture with satellite data. The adjustment scheme for lower and upper temperatures in GDD calculation would account for these larger gaps in spring time. It has become constant with R values more than 0.7 since DOY_{145} of all 8-d periods in ten years. From the above, our result gives a powerful demonstration of the capability to employ remotely sensed AGDD to assess the accumulative heat condition in later rice growing season.

3.4 Using MODIS-derived indices to evaluate the rice growing season heat accumulation

3.4.1 Comparing 2001–2010 spatial and temporal variabilities of heat accumulation

AGDD at DOY_{273} of 8-d period in this paper (equal daily GDD accumulation from DOY_{105}–DOY_{280}) represents the accumulative temperature conditions during all stages of rice growth in Jilin Province. The detailed statistics of the heat accumulation for 10 years were displayed in Table 6. The accumulated heat derived from MODIS data was basically consistent with the calculated value from T_a from meteorological stations. Overall, 10-year correlation coefficient R value between two categories AGDDs ranged from 0.73 to 0.86, which were all above the 0.01 significant levels. This indicates that there was an underestimation of MODIS-derived AGDDs from meteorological AGDDs with 10-year average MBE of 156.75 °C·d, amounting to almost 10% of the relative error. This result can be explained by the underestimation of T_{max} and T_{min} in the later growing season, especially in the fall (Fig. 5). The RMSE of 10 years spans from 143.91 to 236.81 °C·d. However, the interannual variation trend of MODIS-derived AGDDs was almost the same with the heat accumulation calculated from meteorological data. We evaluated this interannual variation by $AGDD_a$; the departure from one-year AGDD to the average of 10 years (Fig. 9). MODIS-derived $AGDD_a$ and meteorological $AGDD_a$ both showed the lower heat accumulation of the years of 2002, 2003, 2005, 2006, and 2009 with negative values, while better heat conditions in 2001, 2007, 2008, and 2010 with positive values. Compared to AGDDs, the correlation between two $AGDD_a$ was less high (only seven years over the significant level) because the multi-year universal models adopted to estimate T_{max}/T_{min} were not ideal for all 10 years. We chose these universal models because they are better at comparing the interannual variation by removing the uncertainty caused by single models, and forecasting the accumulative heat resource in the later year without using meteorological data.

An illustration of AGDD anomaly maps at 1 km spatial resolution was produced for the 2001–2010

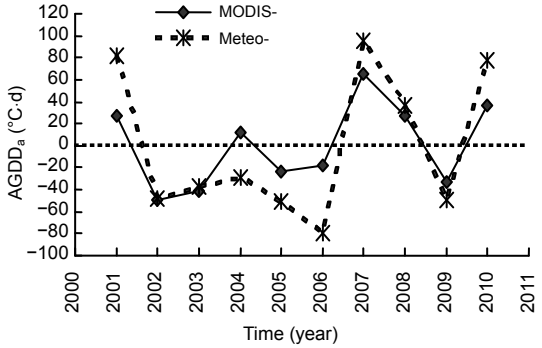

Fig. 9 Comparison of MODIS-derived and meteorological DOY_{273} AGDD anomalies from 2001 to 2010
The dotted line stands for the "0" value line

Table 6 Correlation coefficients and error statistics (MBE, MAE, and RMSE) of $DOY_{105–280}$ AGDDs derived from MODIS data and meteorological stations from 2001 to 2010

Year	AGDD (°C·d)					R
	MODIS-	Meteo-	MBE	MAE	RMSE	
2001	1392.83	1606.07	212.6	215.79	236.81	0.83**
2002	1316.88	1475.8	157.46	163.6	185.69	0.83**
2003	1324.22	1486.85	161.91	163.21	183.38	0.86**
2004	1378.04	1495.24	116.66	125.51	148.17	0.83**
2005	1342.71	1473.63	129.74	140.34	166.43	0.74**
2006	1347.43	1444.71	95.8	117.59	143.91	0.73**
2007	1430.78	1619.27	187.92	187.92	212.79	0.84**
2008	1392.51	1560.83	166.38	168.85	193.76	0.75**
2009	1332.6	1474.02	140.7	145.74	170.28	0.80**
2010	1402.99	1601.72	198.28	199.18	222.14	0.77**
Mean	1366.10	1523.81	156.75	162.77	186.34	0.80**

** Significance at $p<0.01$

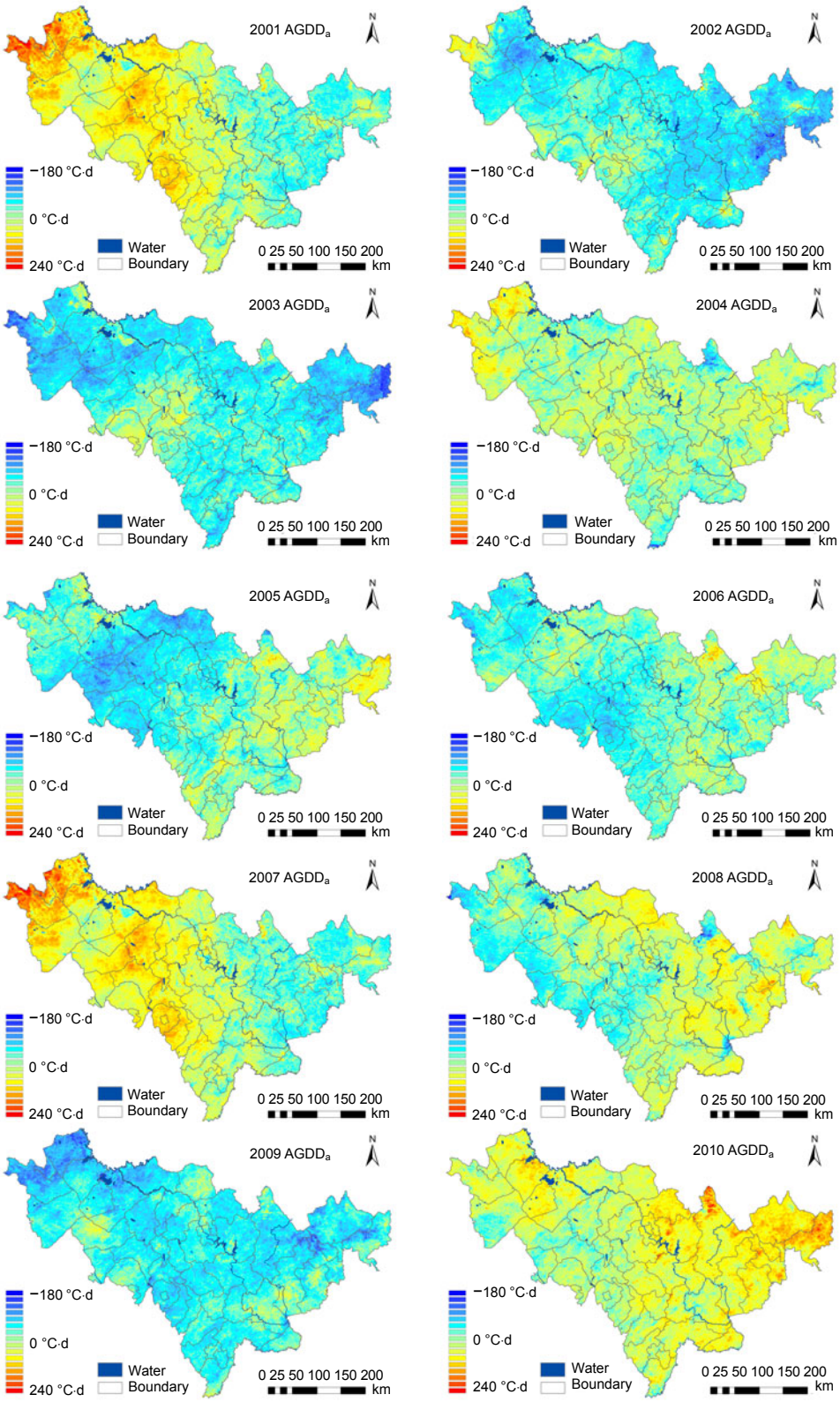

Fig. 10 Spatial distribution of the AGDD anomalies for Jilin Province of rice growing season from 2001 to 2010

The positive AGDD anomalies with warm colors (red, orange) indicate a greater heat accumulation of specified year than the normal level based on the average of the recent 10 years. Vice versa, the negative AGDD anomalies represented in cool color (light and dark blue) mean lower heat accumulation where there is probably a growth delay for rice reaching harvest

period in Jilin Province and is displayed in Fig. 10. Based on this we could characterize the spatial and temporal variability in heat accumulation during the whole rice growing season (AGDD at DOY_{273}) at a large spatial scale year to year. The positive AGDD anomalies with warm colours (red, orange) indicated a greater heat accumulation in a specified year than the normal level based on the average of the recent 10 years. This is usually an indicator above average crop development. Vice versa, the negative AGDD anomalies represented in cool colours (light and dark blue) mean lower heat accumulation and probably indicate areas where below-average rice growth delayed harvest. A similar method of employing AGDD anomalies for corn growth monitoring was found by the North Dakota Agricultural Weather Network. Our results revealed a better overall heat condition for rice cropping in the years of 2001, 2007, and 2010 versus lower heat accumulation in the 2002, 2003, and 2009 years. This characterization was almost the same as the reports of annual analysis of Jilin Agro-meteorological conditions and their impacts on crop production which has been released by the Jilin Provincial Meteorological Bureau.

3.4.2 Estimating GDDs and AGDDs by only using MODIS data

Only MODIS data for 2011 were chosen to evaluate the estimating ability of MODIS indices (GDD, AGDD) to reflect the true ground heat condition without T_a data being taken to be modeled. A total of 44 maximum and minimum T_a maps of each 8-d period of 2011 were calculated by employing the 12 T_a-LST regression models built by 2001–2010 data sets (Table 2) and then spatio-temporal reconstruction.

The average discrepancies between MODIS reconstructed T_a, GDDs, AGDDs and corresponding meteorological values were compared in the forms of MBE, MAE, RMSE, and R (Table 7). The statistical results including all the data pairs from the 50 meteorological stations spanning the 22 8-d periods in rice growing season. Seasonal comparisons between MODIS-derived values and the meteorological estmation for T_{max}, T_{min}, 8-d summated GDDs and every 8-d intervals AGDDs of 2011 are listed in Table 7. Almost all of the correlation of two categories of data for three seasons and four indices are over the 0.01 significant levels except for the T_{max} in summer time (R=0.32). The annual average MAEs of T_{min} and $T_{a\text{-}min}$ in 2011 were 2.386 and 1.829 °C, respectively, slightly larger than those results of 2001–2010. Point-samples of MODIS-derived GDD and AGDD values were compared against the meteorological values; high R values were found with 0.91 for GDD and 0.99 for AGDD.

The scatter plots of all data pairs in 50 meteorological stations of 22 8-d period during the growing season (total 1100 pairs) of 8-d GDDs and AGDD were displayed in Figs. 11a and 11b, respectively. Compared with the correlation coefficient of 8-d GDDs with R^2 of 0.82, there was a much higher correlation between two AGDDs data sets with R^2 of 0.98. The discrepancies derived from remotely sensed data in real-time monitoring could be reduced to some extend in the long process of accumulation. In conclusion, methodology of estimating remotely sensed accumulative heat time from MODIS data proposed by this current paper is feasible to reflect the ground true heat condition. This would be an advanced replacement of raster maps of such agro-meteorological indices interpolated from meteorological data with GIS.

Except for the quantitative analysis, the spatial pattern of AGDD of the rice growing season in 2011 was validated by the GIS interpolation of meteorological AGDD from 50 ground stations by employing the algorithm proposed by Li *et al*. (2010) (Fig. 12).

Table 7 Seasonality comparisons of discrepancy between MODIS-derived T_a, 8-d GDDs, AGDD, and corresponding true ground values from meteorological stations

Season	T_{max} (°C)				T_{min} (°C)				GDD (°C·d)				AGDD (°C·d)			
	MBE	MAE	RMSE	R	MBE	MAE	RMSE	R	MBE	MAE	RMSE	R	MBE	MAE	RMSE	R
Spring	−0.05	2.65	3.37	0.67	0.55	1.55	2.11	0.88	0.82	11.67	15.36	0.73	−15.28	24.69	31.07	0.92
Summer	1.51	2.26	2.79	0.32	1.31	2.01	2.48	0.70	11.31	15.86	19.24	0.60	42.06	67.73	92.45	0.98
Fall	1.59	2.35	2.85	0.73	0.68	1.78	2.14	0.89	8.74	11.78	15.39	0.74	169.22	169.60	194.58	0.82
Year	1.10	2.39	2.96	0.86	0.96	1.83	2.31	0.94	7.86	13.79	17.33	0.91	55.32	79.15	114.11	0.99

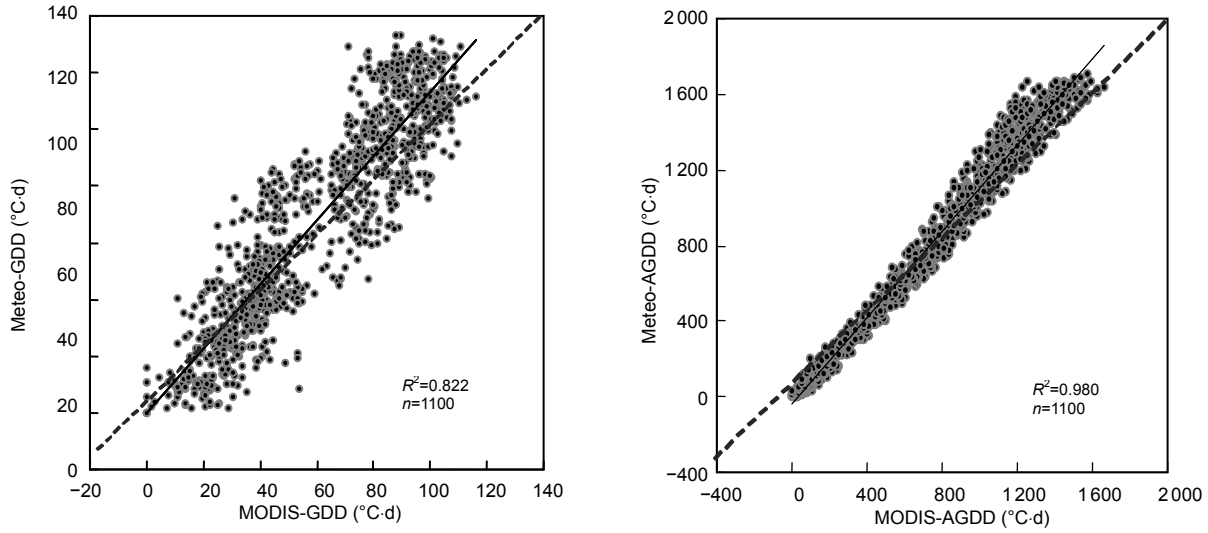

Fig. 11 Scatter plot of 8-d GDDs (a) and scatter plot of AGDD (b) of each 8-d period in whole rice growing season of 2011

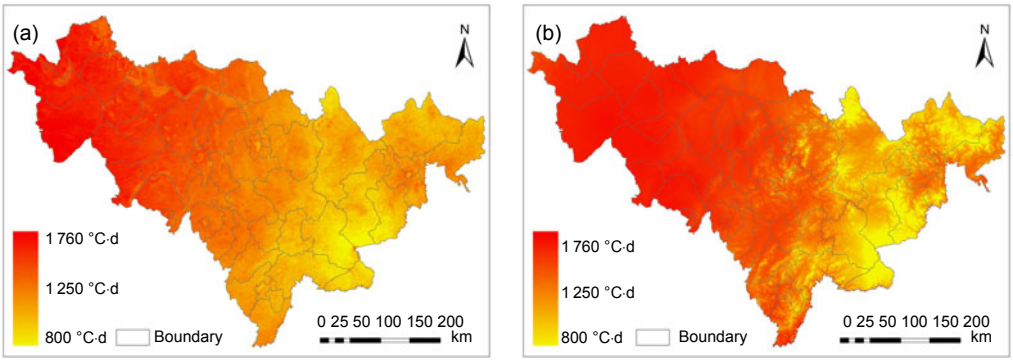

Fig. 12 Spatial distribution of AGDD of rice growing season of Jilin Province in 2011
(a) MODIS-derived; (b) GIS interpolation based on IDW method improved by DEM

Nearly the same spatial distribution of heat accumulation of the rice growing season was shown in the two images. Compared with the traditional GIS interpolation method, remotely sensed accumulative heat estimation exhibited better performance in characterizing microclimates and spatial continuity. This was particularly evident in the northwestern and southeastern parts of the study region.

4 Discussion and conclusions

Estimation of air temperature and filling in missing values due to clouds and low quality pixels are the main critical issues in GDD mapping by satellite data. To solve the problems above, we first adopt the classical multi-regression model to estimate the maximum and minimum T_a from LST images, and then implement a novel spatio-temporal algorithm that combines the temporal merging MODIS LST-based T_a maps at four different acquired times from the Terra and Aqua platform with spatial interpolation based on the temperature gradient with elevation change. The reconstructed T_a images were then used to map agro-meteorological indices expressed in GDDs and AGDDs. When compared with the traditional estimation of ground agro-meteorological indices from the limited number of meteorological stations, remotely sensed accumulative heat estimation exhibits superior performance in microclimates.

In this paper, MODIS 8-d composite LST products (MOD11A2) were demonstrated to be a feasible approach to mapping the heat accumulation for the crop growing season at the regional scale. The

statistical analysis reveals high correlations, over the 0.01 significant level of agro-meteorological indices (GDDs and AGDDs), between estimates from meteorological stations and MODIS LST data.

However, the discrepancy between MODIS-derived AGDDs and ground-derived true values becomes a little large in the later stages of the growing season. GDD is designed to be calculated by daily maximum and minimum T_a and AGDD is the summation of daily GDD. Therefore, 8-d accumulated GDD calculated with 8-d average GDD would lead to more errors in GDD and AGDD estimation comparing with the summation of eight actual daily GDDs. A crucial avenue for further research concerns the reconstruction of daily LST-based T_a estimation for cloudy days, which to some extent can improve the accuracy of remotely sensed GDDs to satisfy the quantified needs of GDD-related remote sensing studies for agriculture and climatology.

Aside from the limited success in applying AGDD and AGDD anomaly map to evaluating the spatio-temporal pattern of heat condition for a whole crop growing season, forecasting future MODIS-derived GDDs and AGDDs with the LST-T_a models constructed by data from previous years was demonstrated to be feasible. Furthermore, it is suggested to employ our methodology to monitor crop growth and identify crop phenological stages by estimating GDDs reaching a certain threshold. Our study may supply a novel approach to heat-related study concerning crop growth monitoring, agricultural climatic regionalization, and agro-meteorological disaster detection at the regional scale.

References

Boschetti, M., Stroppiana, D., Brivio, P.A., Bocchi, S., 2009. Multi-year monitoring of rice crop phenology through time series analysis of MODIS images. *Int. J. Remote Sens.*, **30**(18):4643-4662. [doi:10.1080/01431160802632249]

Coops, N., Duro, D., Wulder, M., Han, T., 2007. Estimating afternoon MODIS land surface temperatures (LST) based on morning MODIS overpass, location and elevation information. *Int. J. Remote Sens.*, **28**(10):2391-2396. [doi:10.1080/01431160701294653]

Cristóbal, J., Ninyerola, M., Pons, X., 2008. Modeling air temperature through a combination of remote sensing and GIS data. *J. Geophys. Res.*, **113**(D13):D13106. [doi:10.1029/2007JD009318]

Crosson, W.L., Al-Hamdan, M.Z., Hemmings, S.N.J., Wade, G.M., 2012. A daily merged MODIS Aqua-Terra land surface temperature data set for the conterminous United States. *Remote Sens. Environ.*, **119**:315-324. [doi:10.1016/j.rse.2011.12.019]

de Beurs, K.M., Henebry, G.M., 2004. Land surface phenology, climatic variation, and institutional change: analyzing agricultural land cover change in Kazakhstan. *Remote Sens. Environ.*, **89**(4):497-509. [doi:10.1016/j.rse.2003.11.006]

de Beurs, K.M., Henebry, G.M., 2010. Spatio-Temporal Statistical Methods for Modelling Land Surface Phenology. Phenological Research: Methods for Environmental and Climate Change Analysis. London, Springer, p.177-208. [doi:10.1007/978-90-481-3335-2_9]

Florio, E., Lele, S., Chang, Y., Sterner, R., Glass, G., 2004. Integrating AVHRR satellite data and NOAA ground observations to predict surface air temperature: a statistical approach. *Int. J. Remote Sens.*, **25**(15):2979-2994. [doi:10.1080/01431160310001624593]

Gordon, R., Bootsma, A., 1993. Analyses of growing degree-days for agriculture in Atlantic Canada. *Clim. Res.*, **3**:169-176. [doi:10.3354/cr003169]

Hassan, Q.K., Bourque, C., Meng, F.R., Richards, W., 2007a. Spatial mapping of growing degree days: an application of MODIS-based surface temperatures and enhanced vegetation index. *J. Appl. Remote Sens.*, **1**(1):013511. [doi:10.1117/1.2740040]

Hassan, Q.K., Bourque, C.P.A., Meng, F.R., 2007b. Application of Landsat-7 ETM$^+$ and MODIS products in mapping seasonal accumulation of growing degree days at an enhanced resolution. *J. Appl. Remote Sens.*, **1**(1):013539. [doi:10.1117/1.2800284]

Huete, A., Didan, K., Miura, T., Rodriguez, E.P., Gao, X., Ferreira, L.G., 2002. Overview of the radiometric and biophysical performance of the MODIS vegetation indices. *Remote Sens. Environ.*, **83**(1-2):195-213. [doi:10.1016/S0034-4257(02)00096-2]

Islam, M., Sikder, S., 2011. Phenology and degree days of rice cultivars under organic culture. *Bangladesh J. Bot.*, **40**(2):149-153.

Ke, L., Wang, Z., Song, C., Lu, Z., 2011. Reconstruction of MODIS LST time series and comparison with land surface temperature (T) among observation stations in the Northeast Qinghai-Tibet plateau. *Prog. Geogr.*, **30**(7):819-826 (in Chinese).

Li, F., Wang, C., Zhao, J., Zheng, J., 2010. The spatialization of multi-year average accumulated temperature in China. *J. Nat. Resour.*, 25(5):778-783 (in Chinese).

Li, J., Wang, X., Ma, W., Zhang, H., 2009. Remote sensing evaluation of urban heat island and its spatial pattern of the Shanghai metropolitan area, China. *Ecol. Complex*, **6**(4):413-420. [doi:10.1016/j.ecocom.2009.02.002]

Liu, J., Wang, Z., Chen, M., Shi, K., Liang, T., Zhang, B., Zhou, F., Chang, J., 2011. Temporal and spatial variation characteristics of effective accumulated temperature in Northeast China during 1951-2007. *J. Anhui Agric. Sci.*, **39**(25):15655-15656, 15680 (in Chinese).

Lu, L., Venus, V., Skidmore, A., Wang, T., Luo, G., 2011. Estimating land-surface temperature under clouds using MSG/SEVIRI observations. *Int. J. Appl. Earth Obs. Geoinform.*, **13**(2):265-276. [doi:10.1016/j.jag.2010.12.007]

McMaster, G.S., Wilhelm, W., 1997. Growing degree-days: one equation, two interpretations. *Agric. For. Meteorol.*, **87**(4):291-300. [doi:10.1016/S0168-1923(97)00027-0]

Morrison, M., McVetty, P., Shaykewich, C., 1989. The determination and verification of a baseline temperature for the growth of Westar summer rape. *Can. J. Plant. Sci.*, **69**(2):455-464. [doi:10.4141/cjps89-057]

Mostovoy, G.V., King, R.L., Reddy, K.R., Kakani, V.G., Filippova, M.G., 2006. Statistical estimation of daily maximum and minimum air temperatures from MODIS LST data over the state of Mississippi. *GISci. Remote Sens.*, **43**(1):78-110. [doi:10.2747/1548-1603.43.1.78]

Neteler, M., 2010. Estimating daily land surface temperatures in mountainous environments by reconstructed MODIS LST data. *Remote Sens.*, **2**(1):333-351 [doi:10.3390/rs1020333]

Sarma, A., Kumar, T.V.L., Koteswararao, K., 2008. Development of an agroclimatic model for the estimation of rice yield. *J. Ind. Geophys. Union*, **12**(2):89-96.

Shen, S., Leptoukh, G.G., 2011. Estimation of surface air temperature over central and eastern Eurasia from MODIS land surface temperature. *Environ. Res. Lett.*, **6**(4):045206. [doi:10.1088/1748-9326/6/4/045206]

Sun, H., Huang, J., Huete, A.R., Peng, D., Zhang, F., 2009. Mapping paddy rice with multi-date moderate-resolution imaging spectroradiometer (MODIS) data in China. *J. Zhejiang Univ.-Sci. A (Appl. Phys. & Eng.)*, **10**(10):1509-1522. [doi:10.1631/jzus.A0820536]

Teal, R., Girma, B., Freeman, K., Arnall, K., Walsh, D.O., Raun, W., 2006. In-season prediction of corn grain yield potential using normalized difference vegetation index. *Agron. J.*, **98**(6):1488. [doi:10.2134/agronj2006.0103]

Vancutsem, C., Ceccato, P., Dinku, T., Connor, S.J., 2010. Evaluation of MODIS land surface temperature data to estimate air temperature in different ecosystems over Africa. *Remote Sens. Environ.*, **114**(2):449-465. [doi:10.1016/j.rse.2009.10.002]

Vina, A., Gitelson, A.A., Rundquist, D.C., Keydan, G.P., Leavitt, B., Schepers, J., 2004. Monitoring maize (*Zea mays* L.) phenology with remote sensing. *Agron. J.*, **96**(4):1139-1147. [doi:10.2134/agronj2004.1139]

Wan, Z., 2007. Collection-5 MODIS Land Surface Temperature Products Users' Guide. ICESS, University of California, Santa Barbara.

Wang, J., Price, K., Rich, P., 2001. Spatial patterns of NDVI in response to precipitation and temperature in the central Great Plains. *J. Appl. Remote Sens.*, **22**(18):3827-3844. [doi:10.1080/01431160010007033]

Yang, W., Yang, L., Merchant, J., 1997. An assessment of AVHRR/NDVI-ecoclimatological relations in Nebraska, USA. *J. Appl. Remote Sens.*, **18**(10):2161-2180. [doi:10.1080/014311697217819]

Ye, Q., Yang, X., Li, Y., Dai, S., Xiao, J., 2011. Changes of China agricultural climate resources under the background of climate change. VIII. Change characteristics of heat resources during the growth period of double cropping rice in Jiangxi Province. *Chin. J. Appl. Ecol.*, **22**(8):2021-2030 (in Chinese).

Zhang, W., Huang, Y., Yu, Y., Sun, W., 2011. Empirical models for estimating daily maximum, minimum and mean air temperatures with MODIS land surface temperatures. *Int. J. Remote Sens.*, **32**(24):9415-9440. [doi:10.1080/01431161.2011.560622]

Zorer, R., Rocchini, D., Delucchi, L., Zottele, F., Meggio, F., Neteler, M., 2011. Use of Multi-annual MODIS Land Surface Temperature Data for the Characterization of the Heat Requirements for Grapevine Varieties. 2011 6th International Workshop on the Analysis of Multi-Temporal Remote Sensing Images, Multi-Temp 2011-Proceedings. IEEE Computer Society, Trento, Italy, p.225-228. [doi:10.1109/Multi-Temp.2011.6005089]